Geometry and Elasticity of Strips and Flowers

M. Marder[1] and N. Papanicolaou[2]

We solve several problems that involve imposing metrics on surfaces. The problem of a strip with a linear metric gradient is formulated in terms of a Lagrangian similar to those used for spin systems. We are able to show that the low energy state of long strips is a twisted helical state like a telephone cord. We then extend the techniques used in this solution to two-dimensional sheets with more general metrics. We find evolution equations and show that when they are not singular, a surface is determined by knowledge of its metric, and the shape of the surface along one line. Finally, we provide numerical evidence by minimizing a suitable energy functional that once these evolution equations become singular, either the surface is not differentiable, or else the metric deviates from the target metric.

KEY WORDS: pattern formation, elasticity, metric, surfaces, differential geometry

1. INTRODUCTION

In 2002, Sharon *et al.* performed experiments by tearing sheets of plastic to produce ruffled edges.[25] The ripping process is quite uniform along the direction of the tear, and the shape that spontaneously results consists in convoluted shapes with much less symmetry than the original deformation. The deformations in the experiments are very large and cannot be treated by any linear theory.

Several papers have already been written on the interpretation of these experiments.[2,3,18−20] They established that one could study the problem by choosing a metric function suggested by the physical process that deformed the sheet, and trying to determine what surfaces were compatible with this metric. Much of the effort in these papers was devoted to exploring the problem of a long thin strip of material with a linear metric gradient in one direction. This strip problem was

---
[1] Center for Nonlinear Dynamics and Department of Physics The University of Texas at Austin, Austin TX 78712, USA; e-mail: marder@chaos.utexas.edu

[2] Department of Physics, University of Crete, and Research Center of Crete, Heraklion, Greece

not solved in generality. Furthermore, the mathematical problem related to the original deformed sheets was not described clearly. On the one hand, the papers spoke of imposing a metric on a sheet, while on the other there were many indications that the actual metric of the final shape adopted by the sheet was something else.

Our goal in this paper is clear up confusions generated in previous discussions of the experiments, and to present some new results on the relation between metrics and surfaces. The three main contributions are

1. We solve completely the strip problem that was defined but only partly solved in Ref. 18
2. We find differential equations suitable to construct surfaces from metrics when such surfaces exist, and construct explicitly some surfaces from the differential equations.
3. We present a variational technique to construct a surface with metric nearby to a desired target metric, even when surfaces with the target metric do not exist.

These three contributions are connected. In Sec. 2 we address the strip problem. We employ Euler angles[12] in a way that allows us to overcome numerical difficulties that had plagued previous approaches. This representation enables us to obtain a complete solution of the problem. Thus, when in Sec. 3 we turn to the more general problem of obtaining surfaces from an arbitrary metric, we use a similar representation and find corresponding numerical advantages. We are able to construct some surfaces explicitly by specifying them along a line and integrating forward with knowledge of the metric alone. However, as we slowly perturb the metric, this procedure breaks down. We show explicitly in Sec. 4 that one can specify target metrics for which no three-dimensional embeddings exist.

A problem very similar to the strip problem we pose in Section 2 has been studied in a series of papers by Goriely, Tabor, and Nizette.[9,10,11,13−15] Most of their papers focus upon dynamical waves traveling on straight strips that have been twisted—a more challenging problem for strips than the one we address. In a particularly pleasing paper on the twisting of tendrils, they also consider strips with spontaneous curvature[14] and find helical solutions such as those we have described. Our contribution to this problem is the finding that putting it into a variational form makes it much easier to solve numerically.

Other questions we consider in this paper are even older. The idea of constructing a surface from a given metric with differential equations goes back to Darboux.[1,16,26] What new do we bring to this topic? We set about the explicit task of constructing surfaces numerically, rather than stopping when a proof of existence has been obtained. There are several things we learn from this process. First, we obtain some new differential equations that are more suitable for

numerical purposes than those of Darboux. In particular, for these differential equations the boundary conditions can be given explicitly, while for Darboux's equations they are determined implicitly. Second, we discover that the vanishing of a denominator that appears both in the Darboux equations and in our variant of them is closely connected with the impossibility of constructing surfaces from certain metrics.

Another line of research with some common elements is shell theory, where numerical methods are far advanced.[4,7,17,23] However, the question normally posed in shell theory is different from the one we have set ourselves. Shell theory presumes an initial surface to be known, and the question is whether it is rigid, and how it responds to small applied stresses or displacements. Our task, instead, is to determine whether surfaces exist at all, and if they do to find them.

2. GROUND STATE FOR TWISTED STRIPS

Reference (24) shows a number of thin strips cut from the edge of a leaf. Each of them curls up into a circle, with the curvature of each strip depending upon the gradient of the metric at that point in the leaf. Such observations suggested that the rippling pattern at the edge of a leaf could be understood by focusing upon a thin strip of material with a metric gradient. Such a strip, freely allowed to seek out its lowest energy state simply curls up into a circle. Therefore the additional constraint was added that the two ends of the strip were constrained to lie separated from each other at a distance λ.[18] This problem yielded nontrivial solutions.[2,18−20] Certain special cases could be found analytically. Somewhat more general solutions could be found numerically. However, the numerical procedures were not very stable, and left open a number of questions. For example, there was some speculation that as the length L of the curved strip became infinite with L/λ kept finite, the lowest-energy state might be fractal. These speculations were incorrect, and deserve to be corrected.

By finding a suitable mathematical representation of this problem, we are able to solve it completely. The final answer is very simple. The lowest energy state of a curled strip whose ends have been pulled apart is a helical shape like a spring. Depending upon exactly where the two ends have been placed, the shape adjusts near the ends to reach required locations and orientations. If the strip is constrained not to exhibit any net twist, it accommodates this requirement through a kink in the middle, with helices of opposite orientation on either side—precisely the solutions described by Goriely and Tabor.[14]

This conclusion seems obvious in retrospect, but it was not so obvious when the problem was first stated, and we therefore explain the steps by which we obtained it. The mathematical representations we employ are generalized and used again in later sections.
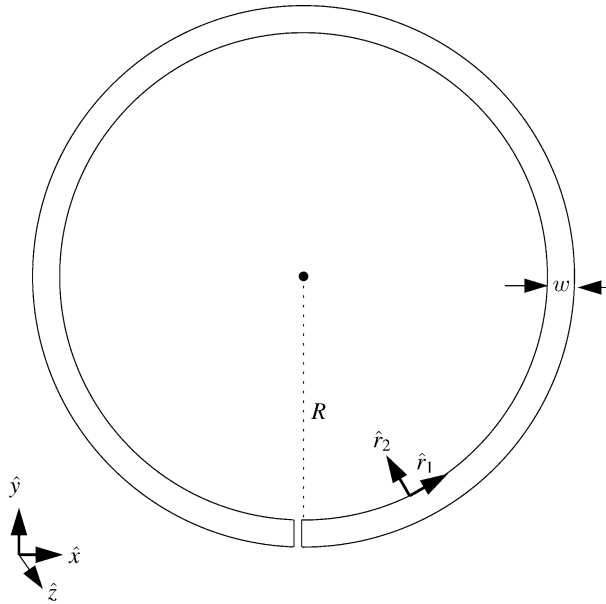
Fig. 1. The buckled strips studied in this section can be examined by cutting out this circular strip, of radius R and width w. Roughly speaking, the main question addressed here is to predict the shape of the strip when the two ends are pulled apart to some specified distance and relative orientation. For the general solutions studied in this section, the total length L of the strip need not equal $2\pi R$.

2.1. Problem Setting

We briefly review the specification of the strip problem. Consider a circular strip of paper, as shown in Fig. 1, of radius R, length $L = 2\pi R$, width w, and thickness t. The length L can be arbitrary, and may be greater or less than $2\pi R$. We will be interested in strips where the following limits apply:

$$\left(\frac{w}{R}\right)^2 \ll \frac{t}{R} \ll \frac{w}{R} \ll \frac{L}{R}. \tag{1}$$

When these conditions hold, the energy of the strip takes a very simple form as a functional of a line passing through the center of the strip.[18]

In particular, let s be the arc length along the center of the strip. The low-energy conformations of the strip are captured by two orthonormal vectors $\hat{r}_1(s)$ and $\hat{r}_2(s)$, where $\hat{r}_1$ points along the arc s, and $\hat{r}_2$ lies in the plane of the strip and is orthogonal to $\hat{r}_1$. Define also $\hat{r}_3 = \hat{r}_1 \times \hat{r}_2$, so as to obtain a set of unit vectors that describes in a natural way the local orientation of the strip. The location $\vec{r}(s)$

of each point along the center-line of the strip can be obtained from

$$\vec{r}(s) = \int_0^s ds' \, \hat{r}_1(s').$$ (2)

At each point s' along the way, the precise orientation of the strip is specified by the unit vector $\hat{r}_2$, or equivalently by the unit vector $\hat{r}_3$, which is normal to the strip. Therefore, the vectors $\hat{r}_1(s)$ and $\hat{r}_2(s)$ contain all the information necessary to deduce the shape of the strip when it is embedded in three-dimensional space. The inequalities (1) ensure that the strip remains essentially flat and featureless in the direction pointing along $\hat{r}_2$.

In terms of the vectors $\hat{r}_1(s)$ and $\hat{r}_2(s)$ the energy of the strip is given by[1,18]

$$U = \int_0^L ds \, \mathcal{E}(s),$$ (3)

where

$$\mathcal{E} = \frac{C_1}{2}(|\hat{r}_1'|^2 - 1/R^2) + \frac{C_2}{2}(|\hat{r}_2'|^2 - 1/R^2),$$ (4)

and primes indicate derivatives with respect to arc length s.

This energy is subject to two constraints. The first is a *local constraint* that results from the fact that the strip has a metric gradient in the direction of $\hat{r}_2$ that causes it to want to curl up with radius of curvature R. This constraint is captured by the condition

$$\hat{r}_1' \cdot \hat{r}_2 = -\hat{r}_2' \cdot \hat{r}_1 = 1/R.$$ (5)

The second constraint is that the ends of the strip be pulled apart by some distance; this constraint prevents the strip from simply curling up into a circle. We impose this constraint through

$$(\vec{r}(L) - \vec{r}(0)) \cdot \hat{z} = \lambda.$$ (6)

That is, the z component of the difference between starting and ending points of the strip is constrained to have value λ. By scanning through values of λ, one equivalently scans through all allowed distances between the starting and ending point of the strip. The constraint in the form of Eq. (6) is much easier to work with formally than if it were literally expressed in terms of end-to-end distance. For definiteness, we choose a fixed (laboratory) frame as shown in Fig. 1. The $\hat{z}$ axis is taken to be perpendicular to the plane defined by the initial (undeformed) circular strip, while the $\hat{x}$ and $\hat{y}$ axes point along the initial directions of $\hat{r}_1$ and $\hat{r}_2$ at one of the endpoints of the strip.

The trihedral $\hat{r}_1, \hat{r}_2, \hat{r}_3$ uses nine coordinates to represent the orientation of the strip, when in fact only three are needed.[12] Further analysis is greatly simplified

by rewriting the unit vectors in terms of Euler angles (Ref. 8 Eq. 4.46), through

$$\hat{r}_1 = [\cos\psi\cos\phi - \cos\theta\sin\phi\sin\psi, \qquad \cos\psi\sin\phi + \cos\theta\cos\phi\sin\psi, \ \sin\theta\sin\psi];$$
$$\hat{r}_2 = [-\sin\psi\cos\phi - \cos\theta\sin\phi\cos\psi, \ -\sin\psi\sin\phi + \cos\theta\cos\phi\cos\psi, \ \sin\theta\cos\psi];$$
$$\hat{r}_3 = [\sin\theta\sin\phi \qquad\qquad\qquad -\sin\theta\cos\phi, \qquad\qquad\qquad \cos\theta].$$
(7)

With this representation, we can rewrite the local constraint Eq. 5 as

$$\cos\theta\,\phi' + \psi' = 1/R;$$
(8)

again, primes refer to derivatives with respect to the arc length s.

Writing out Eq. (4) in terms of the Euler angles one has

$$\begin{aligned}
\mathcal{E} = \frac{1}{2}&\left[(C_2 - C_1)\cos^2\psi + C_1\right]\theta'^2 \\
&+ (C_2 - C_1)\cos\psi\sin\psi\sin\theta\,\phi'\theta' \\
&+ \frac{1}{2}\left[(C_1 - C_2)\cos^2\psi + C_2\right]\sin^2\theta\,\phi'^2.
\end{aligned}$$
(9)

In order to impose the global constraint Eq. (6), we will employ a Lagrange multiplier, and write down the Lagrangian

$$\begin{aligned}
\mathcal{L} = \frac{1}{2}&\left[(C_2 - C_1)\cos^2\psi + C_1\right]\theta'^2 \\
&+ (C_2 - C_1)\cos\psi\sin\psi\sin\theta\,\phi'\theta' \\
&+ \frac{1}{2}\left[(C_1 - C_2)\cos^2\psi + C_2\right]\sin^2\theta\,\phi'^2 \\
&- h\sin\psi\sin\theta.
\end{aligned}$$
(10)

Note that ϕ' appears in Eq. (10), but not ϕ itself. This fact will allow for further simplification.

The constants C_1 and C_2 depend upon elastic properties of the strip. For a particular case studied in Ref. 19, they are related through $2C_2 = 3C_1$. Materials with different elastic properties would give different constants, so we take C_1 and C_2 as free variables. The structure of the equations is particularly simple when $C_1 = C_2$, so we will begin with that case, and return later to the more general situation.

Adopting $C_1 = C_2 = 1$, the Lagrangian of Eq. (10) simplifies to

$$\mathcal{L} = \frac{1}{2}\theta'^2 + \frac{1}{2}\phi'^2\sin^2\theta - h\sin\psi\sin\theta.$$
(11)

All appearances of ϕ can now be eliminated by employing the local constraint Eq. (8) to give

$$\mathcal{L} = \frac{1}{2}\theta'^2 + \frac{1}{2}(\psi' - 1/R)^2 \tan^2\theta - h\sin\psi\sin\theta. \tag{12}$$

Similar Lagrangians appear in the study of spin systems.[5] The equations of motion following from Eq. (12) are

$$[(\psi' - 1/R)\tan^2\theta]' = -h\cos\psi\sin\theta \tag{13}$$

$$\theta'' = (\psi' - 1/R)^2 \frac{\sin\theta}{\cos^3\theta} - h\sin\psi\cos\theta. \tag{14}$$

2.2. Particular Solution

Reference 18 provided a family of exact solutions, and we search for these again with this new formalism. We find that they emerge if one sets $h = 0$. In this case, one immediately integrates Eq. (13) to obtain

$$(\psi' - 1/R)\tan^2\theta = \beta, \tag{15}$$

where β is an integration constant. Inserting this relation into Eq. (14) and integrating gives

$$\theta' = \sqrt{\alpha^2 - \beta^2/\sin^2\theta}$$
$$\Rightarrow \cos\theta = -\sqrt{1 - (\beta/\alpha)^2}\sin(\alpha s), \tag{16}$$

where α is an additional integration constant. Without loss of generality one can choose $\alpha > 0$. Note from Eq. (16) that $\alpha > \beta$ if the solutions are to remain real.

For ψ one obtains

$$\psi = \tan^{-1}((\beta/\alpha)\tan(\alpha s)) - (\beta - 1/R)s + \psi_0. \tag{17}$$

Similarly, for ϕ one obtains

$$\phi = -\tan^{-1}(\sqrt{(\alpha/\beta)^2 - 1}\cos(\alpha s)) + \phi_0; \tag{18}$$

the integration constants ψ_0 and ϕ_0 give the value of ψ and ϕ when $s = 0$.

The global constraint Eq. (6) requires that

$$\int_0^L ds\,\sin\theta\sin\psi = \lambda. \tag{19}$$

As λ becomes large, it is only possible to satisfy Eq. (19) if $\sin\theta$ and $\sin\psi$ have the same period. Comparing Eqs. (17) and (16), one sees that this condition can

be satisfied by taking

$$\beta = \alpha + 1/R. \tag{20}$$

With this choice, one has

$$\sin\theta \sin\psi = \hat{r}_1 \cdot \hat{z} = (\alpha R + \sin^2(\alpha s))/(\alpha R), \tag{21}$$

which with a bit of manipulation upon setting $R = 1$ reproduces Eq. (41a) in Ref. 18. Note that the x axis in that reference corresponds to the z axis here. The remainder of the special solution obtained previously can be recovered as well. Since this special solution depends upon setting $h = 0$, or equivalently to fixing a relationship between λ and L not required by the original problem, we move to a numerical approach capable of solving the problem in greater generality.

2.3. Numerical Solutions

We can obtain reliable numerical ground states of Eq. (11) by changing the form of the Lagrange multiplier to enforce the global constraint in a fashion that involves a positive definite functional:

$$F = \int_0^L ds \left[\frac{1}{2}\theta'^2 + \frac{1}{2}(\psi' - 1/R)^2 \tan^2\theta \right]$$

$$+ H\left(\lambda - \int_0^L ds \, \sin\psi \sin\theta \right)^2, \tag{22}$$

where H is chosen on the order of 100. To find solutions, we simply minimize F.

In the minimization procedure we fix boundary conditions on θ and ψ at $s = 0$ and $s = L$. We may also choose the initial ($s = 0$) value of ϕ, but its final ($s = L$) value is left free to adjust according to Eq. (8). Now we keep one of the endpoints of the strip fixed and orient corresponding initial directions of $\hat{r}_1$ and $\hat{r}_2$ along the $\hat{x}$ and $\hat{y}$ axes of the laboratory frame. Noting that when $\theta = 0$, the orientation of the trihedral depends only upon $\phi + \psi$, the initial values of the Euler angles are set at

$$\theta(0) = 0, \quad \psi(0) + \phi(0) = 0. \tag{23}$$

At the other endpoint, the values of θ and ψ are chosen arbitrarily; e.g.,

$$\theta(L) = \pi/3, \quad \psi(L) = \pi/4, \tag{24}$$

while the end-to-end distance is controlled by the parameter λ. A numerical solution for $L = 13$ and $\lambda = 0.75L$ yields values for θ and ψ shown in Fig. 2. The angle $\phi = \phi(s)$ is obtained by an elementary integration of Eq. (8), and the complete orthonormal trihedral from Eq. (7). It is then straightforward to calculate
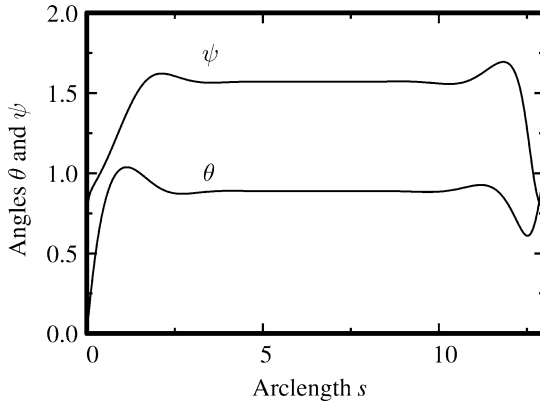
Fig. 2. Plot of Euler angles θ and ϕ for system with total length $L = 13$, constrained to have height in $\hat{z}$ direction $\lambda = .75L$. Note that apart from some variation near the endpoints needed to obey the boundary conditions, both angles go to constant values throughout most of the length of the sample.

$\vec{r} = \vec{r}(s)$ from Eq. (2) which determines the relative position of the strip in three-dimensional space, as illustrated in Fig. 3(a).

One property of the solution that might seem unsatisfactory is that the strip wraps a number of times around the $\hat{z}$ axis. If one were to grab two ends of a strip and pull them apart, this would not be allowed. If one wants to find energy-minimizing solutions without any net twist around the vertical axis, the following strategy is effective: Take a solution obeying the boundary conditions

$$\theta(L) = \pi/2, \quad \psi(L) = \pi/2, \tag{25}$$

produce a mirror image with $z \to -z$, $x \to x$, $y \to y$. The resulting function also minimizes the functional F. It can be glued on to the solution found so far, joining smoothly to it at $s = L$ because of Eq. (25), and will continue on to terminate at $(0, 0, 2\lambda)$ when $s = 2L$. The second half of the solution reverses the twist produced by the first half. In all cases we have checked, solutions of this type are the lowest-energy solutions without net twist.

A notable feature of Fig. 2 and others like it is that the angles θ and ψ quickly approach constant values away from the endpoints, which do not depend on the specific boundary conditions (23) and (24). Thus we conclude that for *long strips*, the energy minimizing solutions have the following properties: θ and ψ are constants such that

$$\sin \psi \sin \theta = \lambda/L, \tag{26}$$

in order to satisfy the global constraint. A physical explanation for this finding is that the system strongly resembles a one-dimensional ferromagnet in an external field.[5] The lowest energy states of such systems involve all spins pointing along
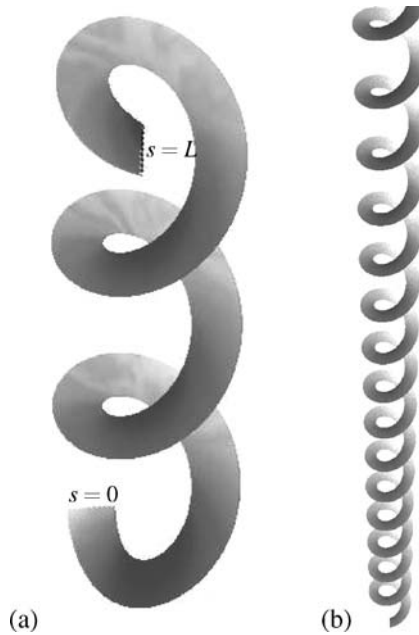
Fig. 3. (a) Three-dimensional visualization of solution shown in Fig. 2. (b) Visualization of low-energy solution for a long strip with $\lambda/L = 0.625$. The strip winds in helical fashion around the $\hat{z}$ axis.

the field. If the ends of the ferromagnet are constrained to point in some different direction, then the ground state is obtained still by having spins point along the field almost everywhere, but at the ends they twist to the imposed direction over a length that is characteristic of the width of domain walls. Our system behaves similarly, and when $C_1 = C_2 = 1$, the width of the boundary region is of order unity.

According to Eq. (13), $\cos \psi \sin \theta = 0$, which is compatible with Eq. (26) only if

$$\psi = \pi/2, \quad \sin \theta = \lambda/L. \tag{27}$$

For solutions obeying Eq. (19), the corresponding energy density

$$\mathcal{E} = \frac{1}{2R^2} \tan^2 \theta = \frac{1}{2R^2} \frac{\lambda^2}{L^2 - \lambda^2} \tag{28}$$

is also constant, independent of s. Nevertheless, the solution oscillates because of Eq. (8), which implies that

$$\phi = \frac{s}{R \cos \theta} = \frac{s}{R\sqrt{1 - (\lambda/L)^2}}. \tag{29}$$

The period of oscillation is given by

$$s_{osc} = 2\pi R \cos\theta = 2\pi R\sqrt{1 - (\lambda/L)^2}. \tag{30}$$

and the distance the solution travels when s traverses this arc-length is

$$z_{osc} = 2\pi R \sin\theta \cos\theta = 2\pi R\sqrt{1 - (\lambda/L)^2}\frac{\lambda}{L}. \tag{31}$$

This last expression gives the period of oscillation one would measure upon taking a strip with $L \gg R$ and pinning its ends at distance λ in the laboratory. A three-dimensional visualization of such a strip appears in Figure 3(b).

Thus we arrive at the conclusion that long strips with metric gradients minimize their energy by curling up like telephone cords. They deviate from this quasi-uniform solution only when they must maneuver near the ends to obey boundary conditions, or form a kink in the middle to produce a solution with no net twist. The problem does not have elaborate pattern-forming solutions.

Returning to the general case where $C_1 \neq C_2$ and writing out the Euler–Lagrange equations, we find that the uniform configuration (27) is still a solution. The energy density is given by $\mathcal{E} = C_2 \tan^2\theta/2R^2$ and all other features of the global minimum such as the period of oscillation remain unchanged.

3. GEOMETRICAL CONSIDERATIONS

The experiments that motivated this work[25] were performed on two-dimensional sheets of deformed material. The logic behind solving the strip problem was that perhaps a two-dimensional sheet could be viewed as the outcome of gluing many strips together in sequence. The results of trying to pursue this idea occupy the rest of the paper. Some parts of the strip problem, such as the representation with Euler angles, can be carried over quite literally. In addition, we found compatibility conditions Sec. (3.2) that generalize the local constraint Eq. (5) into two dimensions.

However, two-dimensional sheets bring into play some long-known difficulties that are not present for the one-dimensional strip. Sometimes when one specifies a metric, a sheet that possesses this metric can be constructed. Sec. 3 is devoted to exploring cases where this occurs, and to discussing the extent to which the surface is determined uniquely. However, sometimes no differentiable sheet with the desired target metric exists. In this case, when one attempts to construct a sheet with the target metric, it inevitably stretches and adopts a slightly different metric. We discuss a numerical procedure capable of exploring surfaces of this type in Sec. 4. One can think of the first type of surface as one that bends but does not need to stretch, and the second type of surface as one that has in-plane stresses that cannot be removed even when it relaxes to its ground state.

As preparation for the study of two-dimensional sheets, we summarize some basic facts concerning the differential geometry of surfaces so as to establish notation and conventions.

Let $\vec{r} = (x, y, z)$ be a point in three-dimensional Euclidean space, where x, y, and z are the usual Cartesian coordinates with respect to a fixed laboratory frame. A surface may then be defined in parametric form by

$$\vec{r} = \vec{r}(u, v) = (x(u, v), y(u, v), z(u, v)) \tag{32}$$

where u and v are parameters whose range is not specified for the moment. Throughout this section, derivatives will be abbreviated by $\partial_1 = \partial/\partial u$ and $\partial_2 = \partial/\partial v$. The elements of the metric tensor are then defined from

$$g_{\alpha\beta} = (\partial_\alpha \vec{r}) \cdot (\partial_\beta \vec{r}). \tag{33}$$

A second fundamental form (tensor) is defined as follows: Let $\hat{r}_3 = \hat{r}_3(u, v)$ be the unit vector that is perpendicular to the surface at point (u, v) and varies continuously with u and v. The elements of the second fundamental form are then given by

$$d_{\alpha\beta} = \hat{r}_3 \cdot \partial_\alpha \partial_\beta \vec{r}. \tag{34}$$

The two symmetric tensors $g_{\alpha\beta}$ and $d_{\alpha\beta}$ play a significant role in the theory of surfaces, as is apparent in standard texts.[6,22]

3.1. Trumpets

In order to gain familiarity with the types of surfaces studied in Sec. 4, we first consider an elementary example defined by

$$\vec{r} = \rho(v)(\cos u \, \hat{e}_1 + \sin u \, \hat{e}_2) + \zeta(v)\hat{e}_3, \tag{35}$$

where $\hat{e}_1$, $\hat{e}_2$, and $\hat{e}_3$ are constant unit vectors along the three axes of the laboratory frame, while $\rho(v)$ and $\zeta(v)$ are functions of v alone, and are further restricted by the condition

$$\rho'^2 + \zeta'^2 = 1, \tag{36}$$

where the primes indicate derivatives with respect to v. The surface is thus specified by the single function $\rho = \rho(v)$. In particular, the metric tensor is then given by

$$g_{11} = \rho^2, \; g_{22} = 1, \; g_{12} = 0. \tag{37}$$

In order to calculate the second fundamental form, we first construct the orthonormal trihedral

$$\hat{r}_1 = \frac{1}{\rho}\partial_1 \vec{r} = -\sin u \, \hat{e}_1 + \cos u \, \hat{e}_2$$

$$\hat{r}_2 = \partial_2 \vec{r} = \rho'(\cos u \hat{e}_1 + \sin u \hat{e}_2) + \sqrt{1 - \rho'^2}\hat{e}_3 \qquad (38)$$

$$\hat{r}_3 = = \sqrt{1 - \rho'^2}(\cos u \hat{e}_1 + \sin u \hat{e}_2) - \rho'\hat{e}_3,$$

where $\hat{r}_1$ and $\hat{r}_2$ are tangent to the surface, while $\hat{r}_3 = \hat{r}_1 \times \hat{r}_2$ is perpendicular. The second fundamental form is then calculated from Eq. (34) to yield

$$d_{11} = -\rho\sqrt{1 - \rho'^2}, \quad d_{22} = \frac{\rho''}{\sqrt{1 - \rho'^2}}$$

$$d_{12} = d_{21} = 0 \qquad (39)$$

A special case of this class of surfaces is the ordinary cylinder with unit radius, obtained with the choice $\rho = 1$ and $\zeta = v$. The metric is then Euclidean ($g_{11} = 1 = g_{22}, g_{12} = g_{21} = 0$) and the elements of the second fundamental form are $d_{11} = -1, d_{22} = 0, d_{12} = d_{21} = 0$.

A more interesting example is obtained by the choice

$$\sqrt{g_{11}} = \rho = 1 + \frac{1}{1 - v}, \qquad (40)$$

which leads to an axially symmetric surface with variable radius $\rho = \rho(v)$ and height $z = \zeta(v)$ calculated from Eq. (36). This surface reduces to the ordinary cylinder in the limit $v \to -\infty$, but its radius increases with increasing v (or z). It would appear that the radius of this surface would eventually grow to infinity as $v \to 1$. Actually, this limit cannot be obtained because of a singularity that develops earlier when $\rho'^2 = 1$ or $v = 0$. The actual surface is illustrated in Fig. 4; we will refer to it as the *trumpet*. It starts as a cylinder with radius $\rho = 1$ and terminates at a cusp with radius $\rho = 2$. Near the cusp the elements of the second fundamental form calculated from Eq. (39) approach the characteristic limits $d_{11} \to 0, d_{22} \to \infty$, while d_{12} vanishes everywhere.

This trumpet may be considered the most primitive model of a flower. However, a true flower is a trumpet that is allowed to grow beyond the cusp, and displays

Fig. 4. Rendering of the surface produced by the metric in Eq. (40) for $u \in [0, 2\pi]$, and $v \in (-\infty, 0]$.

numerous ripples, because biology and elasticity dictate slight modifications of the metric and second fundamental form needed to evade the singularity. Geometry alone cannot resolve what happens as one tries to push a surface beyond such a cusp, but may help to classify the possibilities.

Hence, in the remainder of this section, we formulate an inverse problem of sorts that will enable us to interpret the explicit results of Sec. 4.

3.2. Compatibility Conditions

In order to interpret experiments on surfaces with distorted metrics, what we would most like to do would be to construct the surface quickly and directly from the metric. We restrict our attention to surfaces for which the coordinate curves form an *orthogonal net*, which means that they are characterized by a metric of the form

$$g_{11} = g_{11}(u, v), \ g_{22} = g_{22}(u, v), \ g_{12} = 0. \tag{41}$$

The more general case can also be treated, but all the calculations are more cumbersome, and are not needed for the examples we have in mind. The corresponding orthonormal trihedral is then defined from

$$\hat{r}_1 = \frac{\partial_1 \vec{r}}{\sqrt{g_{11}}}, \ \hat{r}_2 = \frac{\partial_2 \vec{r}}{\sqrt{g_{22}}}, \ \hat{r}_3 = \hat{r}_1 \times \hat{r}_2. \tag{42}$$

We now consider the elementary integrability condition

$$\partial_1 \partial_2 \vec{r} = \partial_2 \partial_1 \vec{r}$$

$$\Rightarrow \partial_1(\sqrt{g_{22}}\hat{r}_2) = \partial_2(\sqrt{g_{11}}\hat{r}_1) \tag{43}$$

$$\Rightarrow (\partial_1 \sqrt{g_{22}})\hat{r}_2 + \sqrt{g_{22}}\partial_1 \hat{r}_2 = (\partial_2 \sqrt{g_{11}})\hat{r}_1 + \sqrt{g_{11}}\partial_2 \hat{r}_1$$

Contracting both sides of Eq. (43) with the unit vectors $\hat{r}_1$, $\hat{r}_2$ and $\hat{r}_3$ in turn we obtain

$$(\hat{r}_1 \cdot \partial_1 \hat{r}_2) = \frac{\partial_2 \sqrt{g_{11}}}{\sqrt{g_{22}}} \tag{44}$$

$$(\hat{r}_2 \cdot \partial_2 \hat{r}_1) = \frac{\partial_1 \sqrt{g_{22}}}{\sqrt{g_{11}}} \tag{45}$$

$$\sqrt{g_{11}}(\hat{r}_3 \cdot \partial_2 \hat{r}_1) = \sqrt{g_{22}}(\hat{r}_3 \cdot \partial_1 \hat{r}_2). \tag{46}$$

We observe that for $\sqrt{g_{11}} = 1 - v/R$, $g_{22} = 1$, Eq. (44) reproduces Eq. (5). As in Sec. 2, we parameterize the trihedral with the Euler angles of Eq. (7) to obtain the three fundamental equations

$$\cos\theta \, \partial_1 \phi + \partial_1 \psi = -\frac{\partial_2 \sqrt{g_{11}}}{\sqrt{g_{22}}} \tag{47}$$

$$\cos\theta \, \partial_2\phi + \partial_2\psi = \frac{\partial_1\sqrt{g_{22}}}{\sqrt{g_{11}}} \tag{48}$$

$$\sqrt{g_{11}}(-\sin\theta\cos\psi \, \partial_2\phi + \sin\psi \, \partial_2\theta)$$
$$= \sqrt{g_{22}}(\sin\theta\sin\psi \, \partial_1\phi + \cos\psi \, \partial_1\theta), \tag{49}$$

which will provide the basis for subsequent development. It should be noted that the compatibility conditions Eqs. (47)–(49) are formulated entirely in terms of the metric tensor $g_{\alpha\beta}$ and that the elements of the second fundamental form do not appear explicitly. In fact, once a solution of Eqs. (47)–(49) is available, $d_{\alpha\beta}$ can be computed from Eq. (34) as

$$\begin{aligned}
d_{11} &= \sqrt{g_{11}}(\hat{r}_3 \cdot \partial_1\hat{r}_1) \\
&= \sqrt{g_{11}}(-\sin\theta\cos\psi \, \partial_1\phi + \sin\psi \, \partial_1\theta) \\
d_{22} &= \sqrt{g_{22}}(\hat{r}_3 \cdot \partial_2\hat{r}_2) \\
&= \sqrt{g_{22}}(\sin\theta\sin\psi \, \partial_2\phi + \cos\psi \, \partial_2\theta) \\
d_{12} &= \sqrt{g_{22}}(\hat{r}_3 \cdot \partial_1\hat{r}_2) \\
&= \sqrt{g_{22}}(\sin\theta\sin\psi \, \partial_1\phi + \cos\psi \, \partial_1\theta) \\
d_{21} &= \sqrt{g_{11}}(\hat{r}_3 \cdot \partial_2\hat{r}_1) \\
&= \sqrt{g_{11}}(-\sin\theta\cos\psi \, \partial_2\phi + \sin\psi \, \partial_2\theta)
\end{aligned} \tag{50}$$

Note that the symmetry condition $d_{12} = d_{21}$ is not explicit in Eqs. (50) but is enforced by Eq. (49).

As an elementary illustration, we return to the case of a trumpet characterized by a metric of the form $\sqrt{g_{11}} = \rho(v)$, $\sqrt{g_{22}} = 1$, and $g_{12} = 0$. It is straightforward to verify that

$$\psi = 0, \; \phi = \pi/2 + u, \; \cos\theta = -\rho', \; \sin\theta = \sqrt{1 - \rho'^2} \tag{51}$$

is a solution of Eqs. (47)–(49) that reproduces the trumpet discussed earlier in this section.

Our aim in Sec. 3.3 is to employ Eqs. (47)–(49) as evolution equations actually to calculate trumpet-like solutions for the general class of metrics given by Eq. (41) through the solution of an initial value problem. Connections with the standard Darboux equation and Gauss–Codazzi compatibility conditions[6,26] are briefly discussed in Sec. 3.4.

3.3. Evolution Equations

Consider the trumpet with metric given by Eq. (40). When $v \to -\infty$, the surface approaches a cylinder. Can one choose some large negative value of v, suppose that the surface for this value of v is a circle, and integrate towards $v = 0$ knowing nothing but the metric and reconstruct the trumpet? The answer is yes. One can find three first-order equations that express the changes of θ, ψ, and ϕ with respect to v and integrate them forward as if v is a time variable. Thus we accomplish the goal of establishing an evolution equation whose boundary conditions require only the shape of a surface along a line.

Finding the equations is not completely straightforward. Eqs. (47)–(49) consist in three first-order partial differential equations for the three Euler angles θ, ψ, and ϕ. However since Eq. (47) involves derivatives in u only, algebraic manipulation alone does not allow one to solve for $\partial_2\theta$, $\partial_2\psi$, and $\partial_2\phi$.

Note that derivatives of ϕ appear in Eqs. (47)–(49) but not ϕ itself. One can use Eqs. (47) and (48) to express $\partial_1\phi$ and $\partial_2\phi$ in terms of the other two Euler angles. Removing ϕ in this way is only permitted, however, if after solving for $\partial_1\phi$ and $\partial_2\phi$ one imposes the condition $\partial_1\partial_2\phi = \partial_2\partial_1\phi$ to obtain

$$(\sqrt{g_{11}\,g_{22}}\partial_1\psi + \sqrt{g_{11}}\partial_2\sqrt{g_{11}})\partial_2\theta - \sqrt{g_{22}}G\cot\theta$$
$$= (\sqrt{g_{11}\,g_{22}}\partial_2\psi - \sqrt{g_{22}}\partial_1\sqrt{g_{22}})\,\partial_1\theta, \tag{52}$$

where

$$G = \frac{\sqrt{g_{11}}}{g_{22}}(\partial_2\sqrt{g_{11}})\,\partial_2\sqrt{g_{22}} + \frac{1}{\sqrt{g_{11}}}(\partial_1\sqrt{g_{11}})\partial_1\sqrt{g_{22}}$$

$$- \partial_1\partial_1\sqrt{g_{22}} - \frac{\sqrt{g_{11}}}{\sqrt{g_{22}}}\partial_2\partial_2\sqrt{g_{11}} \tag{53}$$

One now solves Eqs. (47)–(49) and Eq. (52) for $\partial_2\theta$, $\partial_2\psi$, $\partial_1\phi$ and $\partial_2\phi$. In expressing the results, it is convenient to use the expressions for the second fundamental form in Eq. (50) as shorthand for combinations of derivatives. One obtains

$$\partial_2\theta = \frac{d_{12}\partial_1\theta + G\cos\psi}{d_{11}} \tag{54}$$

$$\partial_2\psi = \frac{1}{d_{11}}\left[\frac{\partial_1\sqrt{g_{22}}}{\sqrt{g_{11}}}d_{11} - \cos\theta\,d_{12}\partial_1\phi - G\sin\psi\cot\theta\right] \tag{55}$$

$$\partial_2\phi = \frac{\partial_1\sqrt{g_{22}}}{\cos\theta\sqrt{g_{11}}} - \frac{\partial_2\psi}{\cos\theta}. \tag{56}$$

These are the basic evolution equations for the Euler angles. Whenever $\partial_1\phi$ appears, it should be viewed as shorthand for

$$\partial_1\phi = -\frac{\sqrt{g_{22}}\partial_1\psi + \partial_2\sqrt{g_{11}}}{\sqrt{g_{22}}\cos\theta}. \tag{57}$$

The procedure for constructing surfaces progresses as follows: We specify the values of θ, ψ, and ϕ for all u and some value of $v = v_0$. To construct a trumpet, we choose v_0 sufficiently negative so that we can use the expressions for cylinder $\psi = 0$, $\phi = \pi/2 + u$, and $\theta = \pi/2$ to set initial values of the Euler angles for $u \in [0, 2\pi]$. Next, we calculate the right hand sides of Eqs. (54) using these initial values, and update each Euler angle through explicit Euler integration, $\theta(v + dv) = \theta(v) + \partial_2\theta\, dv$. It is easy to construct the surface $\vec{r}$. To do so, form the trihedral from the Euler angles through Eq. (7). Then from Eq. (42) one has

$$\partial_2\vec{r} = \sqrt{g_{22}}\hat{r}_2, \tag{58}$$

which means that if the surface is specified on the line $v = v_0$, its future evolution can be determined as well.

The integration process is extremely rapid. We have used it in order to reproduce the trumpet depicted in Fig. 4. The process of integrating forward terminates at $v = 0$ because d_{11} vanishes there for all u, and two denominators in Eqs. (54) become singular.

We have also used the equations to generate surfaces from more general metrics, and a characteristic result is exhibited in Fig. 5. Here we chose the metric

$$\sqrt{g_{11}} = 1 + \frac{1}{1 - v}\left(1 + \frac{1}{2}\cos 3u\right); \; g_{22} = 1. \tag{59}$$

The surface has a slight three-fold modulation that is quite clear if one plots Euler angles, but rather faint when one looks at the surface itself. As in the case of the trumpet, the integration process stops near to $v = 0$. Examining the reason, one

Fig. 5. Three-fold trumpet produced by integrating Eqs. (54) forward from a cylindrically symmetric initial condition at $v_0 = -2\pi$, using the metric in Eq. (59).

finds that once again d_{11} vanishes. This three-fold trumpet does not have cylindrical symmetry, and d_{11} does not vanish simultaneously for all u. Instead, it first vanishes for three values of u. However, the evolution equations are singular and cannot be integrated past this point. Our original hope had been to use evolution equations to obtain flower-like solutions such as the one displayed in Fig. 8. Unfortunately, the rippling edge necessarily involves an oscillation in curvature, and d_{11} must oscillate in sign where ripples are visible. Thus our integration procedure is intrinsically unable to obtain solutions of this type. However, through trials with the evolution equations, we have found that they successfully create surfaces over ranges of u and v where d_{11} does not vanish.

We note in closing that it is not difficult to generalize the equations of this section to the case where $g_{12} \neq 0$. One takes

$$\hat{r}_2 = \frac{\partial_2 \vec{r}/\sqrt{g_{22}} - (\hat{r}_1/\sqrt{g_{22}})\partial_2 \vec{r} \cdot \hat{r}_1}{\sqrt{1 - g_{12}^2/g_{11}g_{22}}} \tag{60}$$

and otherwise proceeds as before. The resulting expressions are lengthy, and as we have not made use of them, we do not record them here.

3.4. Gauss-Codazzi and Darboux

Our treatment has been based upon the compatibility conditions Eq. (43) which are formulated purely in terms of the metric tensor $g_{\alpha\beta}$, while the second fundamental tensor is a derived quantity displayed in Eq. (50). By contrast, both tensors $g_{\alpha\beta}$ and $d_{\alpha\beta}$ appear as fundamental variables in the formulation of the Gauss–Codazzi compatibility conditions employed in standard treatments.[6] It would then be interesting to demonstrate that the Gauss–Codazzi equations can actually be derived starting from the compatibility conditions Eq. (43) and the definitions Eq. (50).

Without going through the laborious calculations needed to establish this equivalence, we merely state here all three Gauss–Codazzi equations in symbolic form:

$$d_{22} = \frac{d_{12}^2 + R_{1212}}{d_{11}}$$

$$\partial_2 d_{11} = \partial_1 d_{12} + d_{1\gamma} \left\{ \begin{matrix} \gamma \\ 12 \end{matrix} \right\} - d_{2\gamma} \left\{ \begin{matrix} \gamma \\ 11 \end{matrix} \right\} \tag{61}$$

$$\partial_2 d_{12} = \partial_1 d_{22} - d_{2\gamma} \left\{ \begin{matrix} \gamma \\ 12 \end{matrix} \right\} + d_{1\gamma} \left\{ \begin{matrix} \gamma \\ 22 \end{matrix} \right\},$$

where $\left\{ \begin{smallmatrix} \gamma \\ \alpha\beta \end{smallmatrix} \right\}$ are the Christoffel symbols. Eqs. (61) are again written in the form of evolution equations and can be solved with initial conditions starting at $v \to -\infty$ given the ordinary cylinder values $d_{11} = -1$, $d_{22} = 0$ and $d_{12} = 0$. Once a solution

of Eqs. (61) is obtained at some finite v, the actual construction of the surface proceeds through the solution of a compatible system of linear equations: see Eqs. (39.8) of Ref. 6.

Finally, we return to the connection between the evolution equations we have derived, and the classic construction due to Darboux and described by Spivak,[26] Chapter 11. Darboux's equation is a second-order differential equation for the height z of a surface as a function of the coordinates u and v. It is hyperbolic or elliptic depending upon the sign of the Gaussian curvature; for the surfaces we consider where the Gaussian curvature is negative, it is hyperbolic. To employ these equations one must provide initial data on z and one derivative along some line. For example, one could integrate the equations and construct a surface if one knew $z(u, 0)$ and $\partial_1 z(u, 0)$ for $u \in [0, 1]$. However, these boundary conditions are not natural, particularly since the components $x(u, 0)$ and $y(u, 0)$ are only determined at the end of the calculation. It is much more natural to begin with the shape of the surface along a line, $x(u, 0)$, $y(u, 0)$, $z(u, 0)$, rather than just one of these components and its derivative, and we showed in Sec. 3.3 how this can be accomplished.

For an orthogonal net, the Darboux equation takes the form

$$\partial_2 z = p$$

$$\partial_2 p = \frac{\left(\partial_1 p - \left\{ {1 \atop 12} \right\} \partial_1 z \right)^2 + R_{1212}[(1 - p^2) - (\partial_1 z)^2/g_{11}]}{\partial_1^2 z - \left\{ {1 \atop 11} \right\} \partial_1 z - \left\{ {2 \atop 11} \right\} p}. \tag{62}$$

From the first of the Gauss formulas (Ref. 26, p. 207) note that the denominator on the right hand side of Eq. (62) is proportional to d_{11}. Therefore the vanishing of d_{11} appears in all formulations to diminish the possibility of evolving surfaces from metrics.

4. GROUND STATE FOR FLOWERS

4.1. Numerical Technique

We now return to techniques employed recently[19] for the construction of surfaces through minimization of an elastic energy functional, and examine again the results in light of what we learned in Sec. 3. We begin by defining more carefully than has been done previously the problem that needs to be solved. In rough outline, one wants to take a thin flat sheet of material, impose a new metric $g_{\alpha\beta}$ upon it, and ask how it deforms in response. A more precise specification of the problem follows:

Differential geometry describes a mapping between two spaces: a reference configuration described by variables (u, v), and a surface described by $\vec{r}(u, v)$.

Experiments on deformed surfaces are performed by taking a flat sheet of material, deforming it in some controlled way, and then allowing the material to buckle in space. To construct a numerical model of the system we will first describe the reference state, corresponding to undeformed material, and then a discrete set of variables that describes a sheet of material moving about in three dimensions.

The experimental reference state consists in a flat slab of material, much wider and longer than it is thick. Imagine therefore positions in a thin sheet described by (x, y, z), where $z \in [0, t]$, and the thickness t is small. Pick N points within this sheet, and label them by $\vec{r}_i^0 = (x_i, y_i, z_i)$, where i ranges from 1 to N. In practice, we will take these points to sit on regular lattices, but they could be randomly distributed. Each point $\vec{r}_i^0$ has a number of near neighbors: label these near neighbors with $j \in n(i)$. Describe the vector between two near neighbors by $\vec{r}_{ij}^0 = \vec{r}_j^0 - \vec{r}_i^0$. We can now write down an energy functional which is constructed precisely so that its ground state gives back this reference configuration. This functional is defined on a new collection of variables $\vec{r}_i$, where again i ranges from 1 to N, and the neighbor list $j \in n(i)$ is the same as in the reference configuration. Now, however, the points $\vec{r}_i$ are free to move anywhere in three-dimensional space. One can think of them as describing arbitrary deformations of the original thin sheet. If a particle i has particle j as a neighbor in the reference configuration, then particle j remains in the list of neighbors no matter how the sheet deforms.

The significance of neighbors is provided by an energy functional that depends upon the squared distance between pairs of neighbors. Define $\vec{r}_{ij} = \vec{r}_j - \vec{r}_i$; then

$$U_0 = \frac{1}{4} \sum_{ij} \left(|\vec{r}_{ij}|^2 - |\vec{r}_{ij}^0|^2 \right)^2. \tag{63}$$

By construction this energy functional has the property that if every particle $\vec{r}_i$ returns to the reference location $\vec{r}_i^0$, then the energy is zero. This ground state is not unique, for the energy is also unchanged if the locations of all the particles are rotated and translated in three-dimensional space, as when one picks up a piece of cardboard and translates and rotates it. Depending upon details involving the numbers of neighbors of each particle, there may be additional degeneracies in the ground state as well, but we will not worry about this point right now.

Our numerical model for deforming the sheet is to go to each bond and stretch it so that the square distance between near neighbors i and j adopts the new value l_{ij}^2. Thus we have the energy functional

$$U = \frac{1}{4} \sum_{ij} \left(|\vec{r}_{ij}|^2 - l_{ij}^2 \right)^2, \tag{64}$$

and direct minimization of U has been employed to obtain most of the three-dimensional figures in this paper.

In order to connect Eq. (64) with the discussion in the previous sections, we must explain the connection between bond lengths l_{ij} and metrics. We use the following prescription. For each bond ij, choose values of u and v through

$$u_{ij} = \hat{e}_1 \cdot (\vec{r}_i^0 + \vec{r}_j^0)/2; \; v_{ij} = \hat{e}_2 \cdot (\vec{r}_i^0 + \vec{r}_j^0)/2. \tag{65}$$

In other words, take u and v to be the x and y coordinates of the midpoints of bonds in the reference configuration. We define a *target metric* through three functions

$$g_{11}^t(u, v), g_{22}^t(u, v), \text{ and } \; g_{12}^t(u, v). \tag{66}$$

One could choose, for example the functions in Eq. (37) if one wanted to recover a trumpet. Using the target metric, one obtains a new equilibrium length squared l_{ij}^2 for the bond between points i and j through

$$l_{ij}^2 = \sum_{\alpha\beta} \vec{r}_{ij}^{0\alpha} g_{\alpha\beta}^t(u_{ij}, v_{ij})\vec{r}_{ij}^{0\beta}. \tag{67}$$

So, for example, if a bond in the reference configuration lies along the x axis at position (u, v) given by Eq. (65), its new length is $\sqrt{g_{11}^t(u, v)}$. The reason that we call $g_{\alpha\beta}^t$ the target metric rather than the metric is that one can put any collection of particle locations one wishes into the functional Eq. (64), not just particle locations that correspond to surfaces with metric $g_{\alpha\beta}^t$. Thus the metric of the surface obtained through numerical minimization may in principle be different from the target. We will be attempting to determine whether the ground states of U produce surfaces whose metric equals the target metric.

One might wonder why U involves squares of bond lengths, rather than $(r_{ij} - l_{ij})^2$. The answer is that Eq. (64) leads to conventional nonlinear elasticity in the continuum limit, while the alternative does not. To obtain the continuum limit, let $\vec{r}(u, v)$ be a continuous vector field, and write

$$\vec{r}_{ij} \approx (\vec{r}_{ij}^0 \cdot \vec{\nabla})\vec{r}. \tag{68}$$

Recalling Eq. (33), substitute Eq. (68) into Eq. (64) to obtain

$$U = \frac{1}{4}\sum_{ij}\left[\sum_{\alpha\beta}\vec{r}_{ij}^{0\alpha}\left(g_{\alpha\beta} - g_{\alpha\beta}^t\right)\vec{r}_{ij}^{0\beta}\right]^2; \tag{69}$$

that is, the energy is given by subtracting the target metric from the actual metric, and vanishes when the two are equal. From Eq. (69) one sees that the appropriate generalization of the Lagrangian strain tensor to situations with target metrics is

$$E_{\alpha\beta} = \frac{1}{2}\left(g_{\alpha\beta} - g_{\alpha\beta}^t\right). \tag{70}$$

If the target metric is a unit tensor, E reduces to the conventional Lagrangian strain tensor of nonlinear elasticity, and when deformations are small it reduces further

to the strain tensor of linear elasticity. One can write

$$U = \sum_{ij} \left[\sum_{\alpha\beta} \vec{r}_{ij}^{\,0\alpha} E_{\alpha\beta} \vec{r}_{ij}^{\,0\beta} \right]^2 . \tag{71}$$

For a particular arrangement of mass points, one can perform the sums over $\vec{r}^{\,0}$ and obtain a specific quadratic functional depending upon the components of E.[19] We do not need these expressions here and will not pursue them further.

However, we will spell out the particular reference configuration $\vec{r}_i^{\,0}$ that has been used to produce results for this paper. It consists in either one or two layers of a triangular lattice. To be completely explicit, use three integers lmn to describe the point locations rather than the single index i:

$$\vec{r}_{lmn}^{\,0} = (1, 0, 0)l + \left(\frac{1}{2}, \frac{\sqrt{3}}{2}, 0 \right) m + \left(\frac{1}{\sqrt{3}}, 0, \sqrt{\frac{2}{3}} \right) n, \tag{72}$$

where l and m range over positive and negative integers, and n equals 0 to produce a single layered structure, or ranges over 0 and 1 to produce a two-layered structure. In the two-layered structure, each particle has nine nearest neighbors, each at unit distance; six with the same value of n on the same horizontal sheet, and three with a different value of n on a different horizontal sheet. In these crystalline structures, the near neighbors of particle i are all the particles j for which $|\vec{r}_{ij}^{\,0}|^2 = 1$.

We record one final technical point about the numerical techniques. Given particle locations $\vec{r}_i$, we will want to view the particles as describing a continuous surface, and to construct its metric. To do so, focus on the lower sheet of particles ($n = 0$ in Eq. (72)) and label the neighbors of particle i as in Fig. 6. Denote by δr_0^2 the square distance from point i to the neighbor located at 0 in the figure and
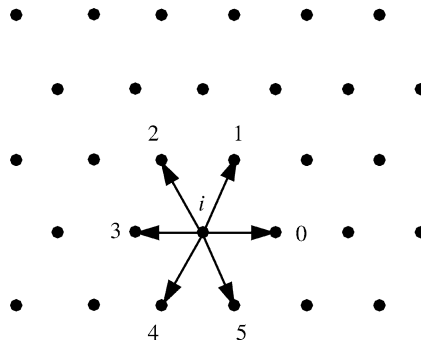
Fig. 6. Enumeration of neighbors surrounding point i, used to describe the construction of numerical metrics in Eq. (74). The diagram shows the particles sitting in the reference configuration $\vec{r}_i^{\,0}$ described by Eq. (72).

so on for the remaining five neighbors. Then we have numerical representations of the metric

$$g_{11} = \frac{\delta r_0^2 + \delta r_3^2}{2}$$

$$g_{22} = \frac{\delta r_1^2 + \delta r_2^2 + \delta r_4^2 + \delta r_5^2 - \delta r_0^2/2 - \delta r_3^2/2}{3}$$

(73)

$$g_{12} = \frac{\delta r_1^2 - \delta r_2^2 - \delta r_4^2 + \delta r_5^2}{2\sqrt{3}}$$

4.2. Numerical Experiments

The questions we wish to pose about target metrics are:

1. What are the ground states of Eq. (69)?
2. When do these ground states correspond to smooth surfaces in the continuum limit?
3. When the ground state is a smooth surface, under what conditions does the target metric equal the metric of the surface?

Observe that ground states of Eq. (69) always exist. The functional is positive definite, and for a finite number of particles must have one or more global minima. If the reference configuration does not have bending stiffness, however, the resulting ground state corresponds to a nondifferentiable surface. To illustrate this point, we use Eq. (40) as a target metric, and work on the domain

$$u \in [0, 2\pi], \quad \text{and} \quad v \in [-3\pi, 0].$$

(74)

We represent the system with a reference crystal 200 columns long, 346 rows high, but only 1 layer thick (in Eq. (72), $l \in [0, 200]$, $m \in [0, 346]$, $n = 0$). Since the reference configuration is infinitely thin, there is no source of bending stiffness. Using the target metric

$$g_{11}^t(u, v) = 1 + \frac{1}{1 - v}$$

$$g_{22}^t(u, v) = 1$$

(75)

$$g_{12}^t(u, v) = 0$$

we minimize U, and the result is displayed in Fig. 7. The total energy U has converged below 10^{-2}, and each bond has reached its target value to better than two parts in 10^4. However, the surface is not smooth, nor is the configuration displayed in the figure plausibly unique. As we know from Sec. 3.1, there do exist smooth surfaces whose metric equals this target metric, but the minimization
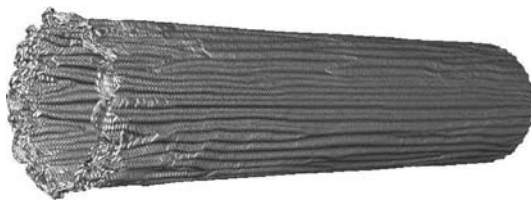
Fig. 7. Image of surface created by minimizing Eq. (69) for a reference crystal with $200 \times 346 \times 1$ particles, and target metric given by Eq. (75). The surface achieves the target; the total energy summed over all particles is less than 10^{-2}. However, the solution is nowhere smooth, and resembles tree bark. It can be understood as an embedding of the target metric whose first derivative is nowhere continuous.

routine under these conditions does not find them. Nash[21] showed that isometric embeddings of 2-surfaces into 3 dimensions exist, but they are not necessarily smooth. Venkataramani *et al.*[27] also discuss non-smooth surfaces of the sort appearing in the figure.

Low energy states of Eq. (69) look very different when one moves from reference crystals with one layer to reference crystals with two layers (In Eq. (72), $n \in [0, 1]$). Now the system possesses some stiffness, and pays an energy penalty for bending too rapidly. Once again minimizing Eq. (69) for the parameter range in Eq. (74), we find the minimum energy state that is essentially the trumpet shown in Fig. 4. The energy of this structure is 74.3; it cannot converge to zero, since springy elastic material has been wrapped into a cylinder.

We compared the metric g as computed through Eq. (74) with the target metric g^t for the structure in Fig. 4. For each metric component, the difference is featureless, and approximately equal to -3×10^{-2} at every point, due to a slight compression needed to bend the inner layer of the reference crystal into a cylinder. We conclude from the numerical calculations that the metric and target metric are equal within numerical accuracy. We emphasize that in Sec. 3.3 we reproduced the trumpet in Fig. 4 through evolution equations; the metric and boundary conditions suffice to determine the surface in this case.

As a more interesting exercise in direct minimization of Eq. (69), we extend the domain beyond the critical point and look for a solution in

$$u \in [0, 2\pi], \quad \text{and} \quad v \in \left[-3\pi, \tfrac{1}{2}\right]. \tag{76}$$

The significance of increasing the range of v is that the theory of Sec. 3.1 is unable to find a smooth surface for $v > 0$. In contrast, upon minimizing U once more, we find the flower-like surface shown in Fig. 8. Now when we subtract the target metric Eq. (75) from the metric actually achieved, Eq. (74), the difference is visible, as shown in Fig. 9. The seven-fold pattern in the surface is reflected in seven-fold oscillations in g_{11} and g_{22}. The off-diagonal component of the tensor, g_{12}, remains zero within numerical accuracy. We conclude that in this case, no
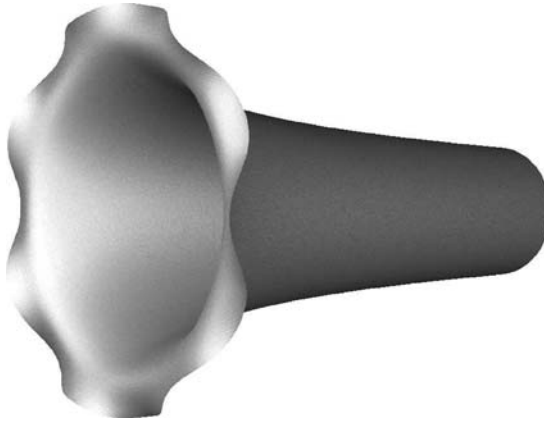
Fig. 8. Image of surface created by minimizing Eq. (69) for a reference crystal with $200 \times 346 \times 2$ particles, and target metric given by Eq. (75), corresponding to a domain where v varies from -3π to $\frac{1}{2}$. Once $v > 0$, trumpet solutions given by Eq. (35) no longer exist, and the evolution equations in Eq. (54) are incapable of finding solutions. The minimum energy state is the smooth flower-like surface with seven-fold symmetry displayed here. As shown in Figure 9, the metric of this surface does not equal the target metric. Creation of this surface required long series of minimizations. The process began by placing particles in a cylinder with a Euclidean metric, and very slowly changing the metric until it reached the desired target value, continually minimizing the functional Eq. (69) along the way. Attempts to find the surface more quickly resulted in higher-energy structures with creases.

smooth surface is able to reproduce the target metric, and numerical minimization finds a metric close to the target that is capable of producing a smooth surface even for $v > 0$. We see no reason that this surface should be considered unique. In all likelihood, its details depend upon the thickness of the sheet. According to Audoly and Boudaoud,[3] one should expect the surface to be increasingly ramified as its thickness diminishes.

As a final exercise, we took the metric components computed numerically and depicted in Fig. 9, inserted them into the evolution equations Eqs. (54) and attempted to reproduce the structure in Fig. 8. This attempt was only partially successful. The evolution equations were unable to proceed past points where d_{11} approached zero. It is clearly possible for d_{11} to vanish without a surface developing singular cusps at that point, but our numerical routines would require very delicate cancellations in order to proceed past such a point.

5. CONCLUSIONS

Given a surface, it is completely straightforward to compute the metric. The inverse problem of finding surfaces compatible with a given metric is much more difficult. In setting out on the studies recorded in this paper, we had two goals.
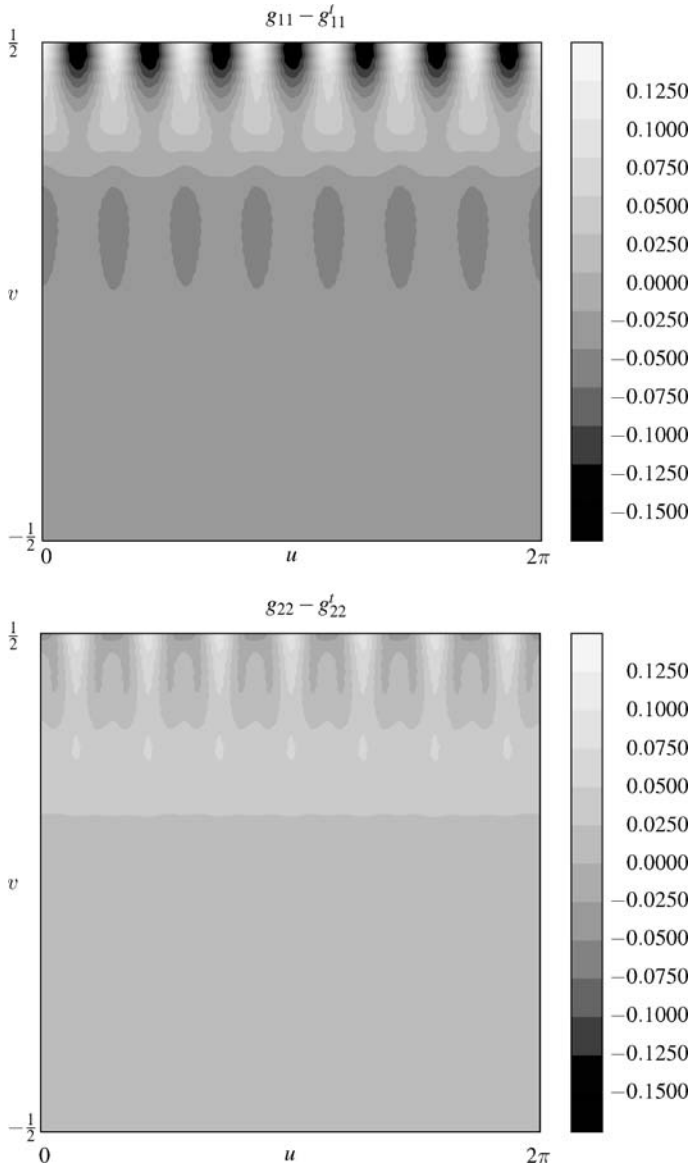
Fig. 9. Metric component deviations for the flower depicted in Fig. 8. Each panel shows a contour plot of the difference between the metric component $g_{\alpha\beta}$ and the target metric $g_{\alpha\beta}^t$. The off-diagonal metric element g_{12} is not illustrated because its numerical values are too small to be discerned at the scale of the figure.

First, we wanted finally to determine the low-energy configurations of long strips with linear gradients in metric. This we have accomplished. Second, we hoped to determine conditions on the relatively simple metrics thought to create the shapes of leaves and flowers[25] that would enable surfaces to be reconstructed.

In the second task we have been only partially successful. We found evolution equations enabling construction of surfaces from initial conditions and metric alone. However, at points when d_{11}, a component of the second fundamental form, vanishes, the equations become singular and cannot be integrated further. We are unable to tell when this singularity really reflects the impossibility of creating a surface compatible with the metric, and when it simply reflects a technical defect in the method of construction.

Some intuitive understanding of this situation can be obtained by thinking about a piece of paper, with flat Euclidean metric. Imagine holding the bottom of the paper completely straight, along the u axis, while the left edge of the paper runs along the v axis. There is an infinite number of shapes the paper can take, which correspond to all different bends possible at different points along v around axes parallel to u. All of these solutions have vanishing curvature in the u direction; $d_{11} = 0$, and the evolution equations (54) accordingly are unable to make any predictions. That is, in some cases the vanishing of d_{11} can correspond to a genuine uncertainty, based upon initial conditions, concerning how the surface should evolve.

On the other hand, for the surface in Fig. 8, the curvature d_{11} oscillates in sign and therefore passes through zero, yet the surface exists. Therefore, the vanishing of d_{11} can be compatible with the existence of a surface even if our purely geometrical methods cannot find it beyond points where $d_{11} = 0$. Minimization of Eq. (64) still produces a surface because elasticity resolves the questions that cannot be answered by geometry.

ACKNOWLEDGMENTS

REFERENCES

1. K. Amano, Global isometric embedding of a Riemannian 2-manifold with nonnegative curvature into a Euclidean 3-space. *J. Diff. Geom.* **34**:49–83 (1991).

2. B. Audoly and A. Boudaoud, Ruban à Godets': an elastic model for ripples in plant leaves. *Comptes Rendus Mecanique* **330**:1–6 (2002).
3. B. Audoly and A. Boudaoud, Self-similar structures near boundaries in strained systems. *Physical Review Letters* **91**:086105/1–4 (2003).
4. D. Chapellet and K. J. Bathe, Fundamental considerations for the finite element analysis of shell structures. *Computers and Structures* **66**:19–36 (1998).
5. J. Chovan, N. Papanicolaou, and S. Komineas, Intermediate phase in the spiral antiferromagnet $Ba_2CuGe_2O_7$. *Physical Review B* **65**:64433 (2002).
6. E. P. Eisenhart, *An Introduction to Differential Geometry, With Use of the Tensor Calculus* (Princeton University Press, Princeton, 1959).
7. A. L. Gol'denveizer, *Theory of elastic thin shells* (ASME, New York, 1961).
8. H. Goldstein, *Classical Mechanics* (Addison–Wesley, Reading, MA, 1969).
9. A. Goriely, M. Nizette and M. Tabor, On the dynamics of elastic strips. *Journal of Nonlinear Science* **11**(1):3–45 (2001).
10. A. Goriely and M. Tabor, Nonlinear dynamics of filaments. 1. Dynamical instabilities. *Physica D* **105**(1–3):20–44 (1997a).
11. A. Goriely and M. Tabor, Nonlinear dynamics of filaments. 2. Nonlinear analysis. *Physica D* **105**(1–3):45–61 (1997b).
12. A. Goriely and M. Tabor, Nonlinear dynamics of filaments. IIIInstabilities of helical rods. *Proceedings of The Royal Society of London Series A-Mathematical Physical and Engineering Sciences* **453**(1967):2583–2601 (1997c).
13. A. Goriely and M. Tabor, Nonlinear dynamics of filaments. IVSpontaneous looping of twisted elastic rods. *Proceedings of the Royal Society of London Series A-Mathematical Physical and Engineering Sciences* **454**(1980), 3183–3202 (1998a).
14. A. Goriely and M. Tabor, Spontaneous helix hand reversal and tendril perversion in climbing plants. *Physical Review Letters* **80**(7):1564–1567 (1998b).
15. A. Goriely and M. Tabor, The nonlinear dynamics of filaments. *Nonlinear Dynamics* **21**(1):101–133 (2000).
16. J. X. Hong, Darboux equations and isometric embedding of Riemannian manifolds with nonnegative curvature in R. *Chinese Annals of Mathematics Series B* **20**:123–136 (1999).
17. J.-L. Lions and E. Sanchez-Palencia, Sensitive boundary value problems. *Comptes Rendus de l'Academie des Sciences, Serie I* **319**:1021–1026 (1994).
18. M. Marder, The shape of the edge of a leaf. cond-mat/0208232 (2002).
19. M. Marder, The shape of the edge of a leaf. *Foundations of Physics* **33**:1743–1768 (2003).
20. M. Marder, E. Sharon, S. Smith, and B. Roman, Theory of edges of leaves. *Europhysics Letters* **62**:498–504 (2003).
21. J. Nash, The imbedding problem for Riemannian manifolds. *Annals of Mathematics* **63**:20–63 (1956).
22. A. V. Pogorelov, *Differential Geometry* (P Noordhoff N. V., Groningen, 1956).
23. E. Sanchez-Palencia, On sensitivity and related phenomena in thin shells which are not geometrically rigid. *Mathematical Models and Methods in Applied Sciences* 139–160 (1999).
24. E. Sharon, M. Marder and H. L. Swinney, Leaves, Flowers and Garbage Bags: Making Waves. *American Scientist* **92**:254–261 (2004).
25. E. Sharon, B. Roman, M. Marder, G.-S. Shin and H. L. Swinney, Buckling Cascades in Free Sheets. *Nature* **419**:579 (2002).
26. M. Spivak, *A Comprehensive Introduction to Differential Geometry*, Vol. 5, second edition (Publish or Perish, Berkeley, 1979).
27. S. Venkataramani, T. Witten, E. Kramer and R. Geroch, Limitations on the smooth confinement of an unstretchable manifold. *Journal of Mathematical Physics* **41**(7):5107–5128 (2000).